Core-Shell CdS-Cu_2S Nanorod Array Solar Cells

Andrew Barnabas Wong [†,‡], Sarah Brittman [†,‡], Yi Yu [†,‡], Neil P. Dasgupta [†,¶], and Peidong Yang [†,‡,⊥,§,]*

[†] Department of Chemistry, University of California, Berkeley, Berkeley, California 94720, United States, [‡]Materials Sciences Division, Lawrence Berkeley National Laboratory, Berkeley, California 94720, United States, [¶]Present address: Department of Mechanical Engineering, University of Michigan, Ann Arbor, Michigan 48109, United States, [⊥]Kavli Energy Nanosciences Institute, Berkeley, California 94720, United States, [§]Department of Materials Science and Engineering, University of California, Berkeley, California 94720, United States

ABSTRACT As an earth-abundant *p-type* semiconductor, copper sulfide (Cu_2S) is an attractive material for application in photovoltaic devices. However, it suffers from a minority carrier diffusion length that is less than the length required for complete light absorption. Core-shell nanowires and nanorods have the potential to alleviate this difficulty because they decouple the length scales of light absorption and charge collection. To achieve this geometry using Cu_2S, cation exchange was applied to an array of CdS nanorods to produce well-defined CdS-Cu_2S core-shell nanorods. Previous work has demonstrated single-nanowire photovoltaic devices from this material system, but in this work, the cation exchange chemistry has been applied to nanorod arrays to produce ensemble-level devices with micro-scale sizes. The core-shell nanorod array devices

show power conversion efficiencies of up to 3.8%. In addition, these devices are stable when measured in air after nearly one month of storage in a desiccator. These results are a first step in the development of large-area nanostructured Cu_2S-based photovoltaics that can be processed from solution.

KEYWORDS: Nanorod Array, Core-Shell, Photovoltaic, Solution Processed, Copper Sulfide

The development of new renewable energy technologies such as photovoltaics for solar energy conversion is an area of considerable interest. From the 1960's through the 1980's, one major approach to produce scalable photovoltaics was the development of thin film CdS/Cu_2S solar cells. In these photovoltaics, the Cu_2S layer serves as an earth-abundant light absorber with an indirect band gap of 1.2 eV,[1] which corresponds to a maximum theoretical efficiency of 30%.[2] To form the heterojunction, the partial conversion of *n*-type cadmium sulfide (CdS) thin films to form *p*-type copper sulfide was performed though a solution phase or solid state cation exchange reaction. In cation exchange, the cations in an initial crystal are replaced with new cations that diffuse into the material from solution. In many cases, the anion lattice is conserved, which allows the initial morphology to be preserved after the reaction.[3-5] This cation exchange chemistry was thought to be a promising route to produce inexpensive and scalable solar cells despite a mismatch between the length scales required for light absorption (~6 μm at 1000 nm for 90% absorption) and diffusion of minority carriers within the Cu_2S (~300 nm).[6] Despite this limitation, rapid progress allowed cell efficiencies to approach 10%,[7] which made this technology competitive with planar silicon-based photovoltaics at the time.[8] Before 1980, the record efficiency for multicrystalline silicon solar cells was only ~15.3%.[9] However, interest in

CdS/Cu_2S waned during the 1980's because of the continued progress of Si solar cells as well as concerns about the long-term stability of CdS/Cu_2S solar cells. Mechanistically, the degradation in performance was thought to occur by the diffusion of Cu^+ into CdS, particularly along grain boundaries, and by oxidation of the Cu_2S at the surface to form non-stoichiometric phases of copper sulfide. [10-12] Recently, there has been progress in the stabilization of Cu_2S for light-harvesting applications through the use of Al_2O_3 protection layers deposited by atomic layer deposition (ALD), [8,12] which partially addresses the stability issues that were previously encountered.

To improve the performance of CdS/Cu_2S solar cells, the core-shell nanowire array geometry is an ideal structure to resolve the mismatch between the short length scale for minority carrier diffusion and the longer length scale for light absorption in Cu_2S by decoupling these directions.[13,14] In addition, nanowires also offer advantages in terms of low optical reflectivity, light trapping, and the potential for flexible, inexpensive, and industrially scalable solar cells.[13,15-22] These advantages may eventually lead to the overall goal of efficient and scalable solution-processed solar cells.

Moreover, core-shell nanowire and nanorod arrays create the opportunity for the synthesis of precise and well-controlled junctions for solar energy conversion. For these reasons, work on Cu_2S and CdS has drawn renewed interest. Cation exchange can produce precisely controlled heteroepitaxial CdS/Cu_2S axial and core-shell junctions in thin nanorods (<15 nm) and nanowires respectively.[14,23,24] These axial nanorod and single nanowire core-shell heteroepitaxial junctions of single-crystalline Cu_2S and CdS have photovoltaic properties without the disadvantage of diffusion along grain boundaries.[14,25] At the level of a single nanowire, CdS-Cu_2S core-shell photovoltaic devices exhibited a record open circuit voltage (0.61 V) and fill factor (80.8%)

compared to all previous Cu_2S/CdS photovoltaics. These values were attributed to the high quality of the CdS/Cu_2S junction formed by performing cation exchange on a single-crystalline CdS wire grown by the vapor-liquid-solid (VLS) mechanism. The CdS-Cu_2S core-shell interface was structurally well defined and heteroepitaxial.[14] Despite this excellent performance, this work presented several new challenges. First, the power output of a single nanowire solar cell is limited; therefore, the assembly of the core-shell nanowires into a scalable device is critical. Second, the shell thickness in these solar cells reached only about 20 nm, which limited the light absorption in the Cu_2S beyond 510 nm and limited short-circuit current densities. To address these challenges, cation exchange chemistry was applied to CdS nanorod arrays patterned with microscale windows to produce solution-processed photovoltaic devices featuring well-defined *p-n* junctions. This approach yields ensemble-level devices in contrast to the previous single-nanowire devices. The vertical array of core-shell nanorods addresses the issue of the mismatched length scales for light absorption and minority carrier diffusion in thin film CdS/Cu_2S devices by decoupling them. Within this vertically oriented array, the Cu_2S shell thickness exceeds 60 nm, which has improved short circuit current density as compared to the previous work on single core-shell nanowires. The micro-scale array devices reach a maximum efficiency of 3.8% and maintain this efficiency after at least one month of storage.

RESULTS AND DISCUSSION

As the CdS substrate for cation exchange, wurtzite CdS nanorods were grown on indium tin oxide (ITO) or fluorine-doped tin oxide (FTO) by modifying a previously reported hydrothermal method.[26,27] At the single nanorod level, transmission electron microscopy (TEM) and selected

area-electron diffraction (SAED) images demonstrate that the nanorods are grown along the c-axis and are single crystalline, which is beneficial for forming a high-quality junction via cation exchange (Figure 1a). Typical nanorods have diameters of 200 to 300 nm and average lengths exceeding 600 nm (Figures 1a, 1b, 1c). The vertical CdS nanorods sit on top of a dense buffer layer that covers the FTO substrate.

Before fabricating the solar cells, cation exchange on the CdS nanorods was found to be able to convert them into Cu_2S either fully or partially, depending on the reaction conditions. Briefly, CdS nanorods were dipped into an aqueous solution of CuCl at 90°C. By controlling reaction time, the synthesis of uniform core-shell nanorods can be achieved through this method, as demonstrated by energy dispersive X-ray spectroscopy (EDS) (Figure 1d). The SAED pattern of a single core-shell CdS-Cu_2S nanorod indicates to formation of crystalline Cu_2S on the CdS shell (Figure 1e). The splitting of the CdS and Cu_2S diffraction spots in the SAED image is due to the difference in d-spacing between the CdS and Cu_2S, and this splitting is an indication of a heteroepitaxial relationship between the CdS in the core and the Cu_2S in the shell in agreement with prior work on core-shell CdS-Cu_2S nanowires. These previous studies have shown that this method of dipping single-crystalline CdS nanowires into the heated aqueous solution forms a heteroepitaxial interface between the CdS core and the rapidly-grown Cu_2S shell.[14,28]

In addition to the formation of core-shell structures, the phase of copper sulfide produced from CdS is also important. It has been shown previously that substoichiometric phases of copper sulfide can be formed from CdS, such as roxbyite ($Cu_{1.74-1.82}S$) and djurleite ($Cu_{1.97-1.93}S$), in addition to stoichiometric low chalcocite (Cu_2S).[24] Planar photovoltaic devices made from copper-deficient phases exhibited lower current densities than devices produced with stoichiometric Cu_2S, and this poorer performance is caused by adverse changes in the absorption coefficient, minority carrier

diffusion length, mobility, and band gap with increasing copper deficiency.[29] As is demonstrated by X-ray diffraction (XRD) in Figure 1f, the core-shell CdS-Cu_2S nanorods formed by cation exchange consist of stoichiometric Cu_2S of the low chalcocite phase, which is most suitable for photovoltaics.

Core-shell nanorod array photovoltaic devices were then fabricated using the CdS-Cu_2S cation exchange reaction as shown in Figure 2a. Briefly, the solution-synthesized CdS nanorod array was coated with a thin layer of Al_2O_3 using ALD and filled with poly(methyl methacrylate) (PMMA) to protect against shunting between the p-type and n-type contacts. Photolithography and O_2 plasma etching were used to define windows with areas of ~25 μm^2 where the devices were fabricated. The PMMA was partially removed with an anisotropic etch to leave only a thin layer of polymer on top of the CdS particles at the bottom of the array (Supporting Information, Figure S1). After the sample was dipped in 10:1 buffered hydrofluoric acid (BHF) solution to remove the Al_2O_3 protection layer, the exposed CdS rods were converted to core-shell CdS-Cu_2S structures to form the junction by dipping the sample into a 90°C aqueous solution of CuCl for 2 to 4 seconds. After cation exchange, the sample was coated with an Al_2O_3 protection layer, and photolithography was used to define the top contact, which consisted of sputtered ITO. A scanning electron microscopy (SEM) image of a representative array device is shown in Figure 2b. The PMMA coating of the buffer layer enables the nanorods to be converted to core-shell structures while the polycrystalline buffer layer remains unconverted, which is illustrated by cross-sectional EDS mapping (Figure 2c). This design prevents the formation of shunt paths from the Cu_2S to the CdS contact. An EDS linescan of a single nanorod shows that the Cu_2S shell thickness used for devices is greater than 60 nm (Figure 2d). The shell thickness can be controlled by the duration of the cation exchange reaction.

The photovoltaic performance of the patterned CdS-Cu_2S nanorod array solar cells was measured under 1-sun conditions (AM 1.5G). The *I-V* characteristic of a champion device exhibited an open circuit voltage of 0.45 V, a short-circuit current density of 12.5 mA/cm^2, and a fill factor of 68.1%, which led to an overall efficiency of 3.8% (Figure 3a). A table of representative devices is shown in the supporting information (Table S2).

The wavelength dependence of the photocurrent reveals that much of the photocurrent arises from wavelengths that are longer than 520 nm (Figure 3b), which is the absorption edge of CdS. This shows that Cu_2S contributes a large fraction of the photocurrent in these devices. There is a dip in the normalized photocurrent around 540 nm, which has been observed in other thin film[1,30] and nanostructured[31] CdS/Cu_2S solar cells. This dip corresponds to the tail of the absorption edge of CdS, wavelengths at which the CdS can be illuminated uniformly to generate holes in the buffer layer that are too far from the interface to be collected.[1] This effect can be particularly pronounced in solar cells that employ light trapping.[1]

Stability of the *I-V* characteristic is also an important consideration because Cu_2S is known to be unstable against oxidation and to exhibit interdiffusion with CdS.[9-11] After devices were fabricated and measured in ambient conditions, the *I-V* characteristic was shown to be stable upon re-measurement 26 days later (Figure 3c) after storage in a desiccator filled with nitrogen under ambient illumination and at room temperature. This is in contrast to previous work on single-crystal thin film CdS/Cu_2S devices, which showed marked degradation even upon storage of the devices in an argon atmosphere, which was attributed to interdiffusion between the CdS and Cu_2S.[11] It is possible that the 1 nm ALD layer on the Cu_2S shell, which is meant to protect the array from oxygen plasma damage during ITO sputtering, may also aid the long term stability, as has been suggested by work on ALD Cu_2S films.[8,12] Another possibility is that the single-

crystalline nanoscale CdS-Cu_2S interface may exhibit increased stability in comparison to the bulk CdS/Cu_2S interface in thin films, which has been suggested previously by TEM studies of the CdS/Cu_2S interface.[32] The heteroepitaxial CdS-Cu_2S interface specifically avoids any potential grain boundary effects by forming heteroepitaxial interfaces only in single-crystalline nanorods. It is possible that the improved stability in these devices relative to thin-film architectures is due to the unique properties of these nanostructured monolithic interfaces, which avoid deleterious effects due to grain boundaries.

Moving forward, several challenges remain to be overcome to achieve large-area nanorod array solar cells that surpass the efficiencies of thin-film CdS/Cu_2S solar cells while maintaining stability. While single-nanowire CdS/Cu_2S solar cells produced open circuit voltages and fill factors greater than those of planar solar cells, these metrics were lower for the nanorod array solar cells. One possible explanation is that the solution-phase-synthesized CdS is more likely to possess defects that facilitate recombination as compared to the nanowires grown at higher temperatures via the VLS-growth mechanism. In principle, this difficulty can be overcome though treatments of the solution-grown CdS such as annealing, which decreases the CdS defect emission in photoluminescence (Supplementary Information Figure, S4). Another possibility is that the band alignment and resulting open circuit voltage between the CdS and Cu_2S are not optimized.

As the maximum current density for Cu_2S is 40 mA/cm^2, improvements still are necessary to approach this limit. As shown in Figure 3b, the wavelength-dependent short-circuit current indicates that many photons absorbed by the CdS-Cu_2S array are not being collected, particularly at wavelengths less than 500 nm. This is in contrast to previous work on the single nanowire core-shell solar cells, which exhibited excellent carrier collection of light for carriers from photons with wavelengths less than 500 nm.[14] A possible explanation for the decreased collection of charges

from light with wavelengths less than 500 nm is that light scattered within the array could be absorbed in the ITO top contact, the FTO underneath the CdS nanorod array, or the CdS buffer layer, where the generated carriers would be too far from the core-shell interfaces to be collected (Supplementary Information, Figure S5).

Scaling up these devices to macroscopic arrays is also an area requiring further investigation. In this study, the size of the active area of the photovoltaic devices was limited by the tendency to form shunt paths during cation exchange when the PMMA protection layer was too thin. If the nanorods were lengthened, it would allow for greater path length for light absorption in the core-shell array, a more robust protection layer, and a reduced portion of light absorbed by the buffer layer of CdS particles. This would improve the scalability and efficiency of these devices.

Lastly, the stability of the CdS/Cu_2S interface within these nanostructures must be investigated more fully. While the preliminary measurement indicating stability after 26 days of storage is promising, further tests investigating the stability under photovoltaic operating conditions are essential.

CONCLUSION

In summary, solution-processed CdS-Cu_2S core-shell nanorod array solar cells have been fabricated and characterized. The champion micro-scale devices have an efficiency of 3.8% and are stable after at least one month of storage. This efficiency approaches that of single nanowire devices and is only a factor of three below the efficiency of the record thin film CdS/Cu_2S devices. As compared to the single nanowire devices previously reported, the current density has been

improved, but the open circuit voltage has been reduced, which is likely related to the material quality. The stability of these photovoltaic devices based on a nanoscale CdS-Cu_2S junction is an area deserving of further study. In terms of future application, many improvements can be made to the core-shell array to enable a more robust protection layer that would allow for larger-area devices. This work represents one step towards the goal of improving the efficiency of photovoltaics through the use of nanostructured absorbers.

METHODS

CdS Nanorod Growth. The growth of CdS nanorods on conductive FTO or ITO substrates was based on a previously reported hydrothermal method.[26,27] CdS nanorods were grown on pre-scored conductive substrates on glass in an autoclave at 200°C for 4 hours. After this reaction, the CdS array was placed back into the autoclave with a fresh stock solution to enlarge the existing nanorods by performing the reaction a second time. The CdS array coated substrates were carefully broken along the pre-scored lines into individual chips of about 1 cm^2. A more detailed description of the CdS array growth is provided in the Supporting Information.

Cation Exchange Reaction. The solution for the cation exchange reaction was prepared in a 25 mL 3-neck flask with 15 mL of 1 M HCl acid. The pH was adjusted to 7 by dropwise addition of hydrazine. An additional 10 mL of deionized water was added. The solution was purged of oxygen by bubbling nitrogen gas throughout the reaction. After a 5 minute purge at room temperature,

heat was applied by a heating mantle to raise the temperature to 90°C. At 50°C, 0.14g of copper (I) chloride (Aldrich, reagent grade >97%) was quickly added to the solution, and the 3-neck flask was resealed. The solution initially had a brown-green appearance that cleared as the copper chloride dissolved. After the temperature stabilized at 90°C, the solution was clear with some grey precipitate. The reaction was opened and CdS arrays were dipped into the solution for 3 to 4 seconds of submerged time followed by rinsing the substrate in deionized water to form the core-shell nanorods. Lower pH and temperature values resulted in changes to the appearance of the solution as well as the reaction rate and the phase as has been described in the case of thin films.[29]

Device Fabrication. The as-grown CdS nanorod arrays were coated in 20 nm of Al_2O_3 at 200°C in a home-built ALD system. After functionalizing the surface with hexamethyldisilazane (HMDS), PMMA (C4, Microchem) was spin coated onto the chip. Within several minutes, the sample was annealed at 120°C for 10 minutes on an equilibrated hotplate. I-line photoresist was then spin coated and baked at 90°C for 90 seconds. The active conversion area was defined using photolithography, and the PMMA was removed from the conversion areas by timed O_2 plasma etching. Active areas fabricated ranged from about 20 to 2500 μm^2. The ALD Al_2O_3 was removed by etching in 10:1 buffered hydrofluoric acid (BHF) solution for 60 seconds followed by annealing at 170°C in Ar for 30 minutes to ensure adhesion of the PMMA to the surface of the CdS after the removal of the Al_2O_3. At this point, cation exchange was performed on these samples. After cation exchange, 1 nm of ALD Al_2O_3 was deposited as a protection layer at 50°C. Afterwards, the HMDS-functionalized surface was coated with I-line photoresist and the area for the contacts was patterned using photolithography. The ITO top contact was deposited by sputtering. To perform liftoff of the ITO, the edges of the sample were carefully scratched, and the chip was soaked for 1

hour in isopropanol before the chip was sonicated for 1-2 seconds to remove excess ITO. Prolonged sonication can induce the formation of high pressure tetragonal phases of Cu_2S.[33] After liftoff, the chips were dried under a stream of nitrogen and annealed in air at 200°C for 5 minutes. Afterwards, devices were stored in nitrogen inside a desiccator (Plas Labs, 862-CGA) under ambient conditions until measurement in air. A more detailed description of the device fabrication is provided in the Supporting Information.

Photovoltaic Device Characterization. Light was provided by a 150W Xenon arc lamp (Newport Corporation) with an AM 1.5 G filter (Newport Corporation). A silicon photodiode referenced to an NREL-calibrated photodiode was used to calibrate the light intensity, and a Keithley 2636 source-measure unit was used to measure the *I-V* characteristic with the entire chip under illumination after carefully contacting the top contact with a soft probe (Picoprobe T-4-22). All measurements were carried out in ambient air. The dependence of the normalized photocurrent on wavelength shown in Figure 3b was obtained by coupling a 300W Xenon arc lamp (Newport Corporation) to a monochromator (Newport Corporation). The photocurrent was measured at 10 nm increments with approximately 15-nm bandwidth, and calibration was carried out using a calibrated silicon photodiode.

Structural Characterization. SEM images were taken using a JEOL JSM-6340F field emission scanning electron microscope. XRD patterns were acquired using a Bruker AXS D8 Advance diffractometer, which used Co Kα radiation with a wavelength of 1.79026 Å. The CdS XRD pattern was indexed to wurtzite CdS (JCSD Card: 01-074-9663), and the Cu_2S XRD pattern was

indexed to low-chalcocite Cu_2S (JCSD Card: 01-073-6145). The ITO was indexed to JCSD Card: 01-089-4596. EDS maps were collected on a FEI Titan microscope operated at 80 kV at the National Center for Electron Microscopy. The microscope was equipped with a FEI Super-X Quad windowless detector based on silicon drift technology controlled by Bruker Esprit software. Cross-sectional samples were prepared by scraping the core-shell nanorod array followed by dry transfer to a Ni TEM grid with a lacey carbon coating. HRTEM images were also taken on the TEAM 0.5 microscope, which was operated at 300kV at the National Center for Electron Microscopy.

FIGURES

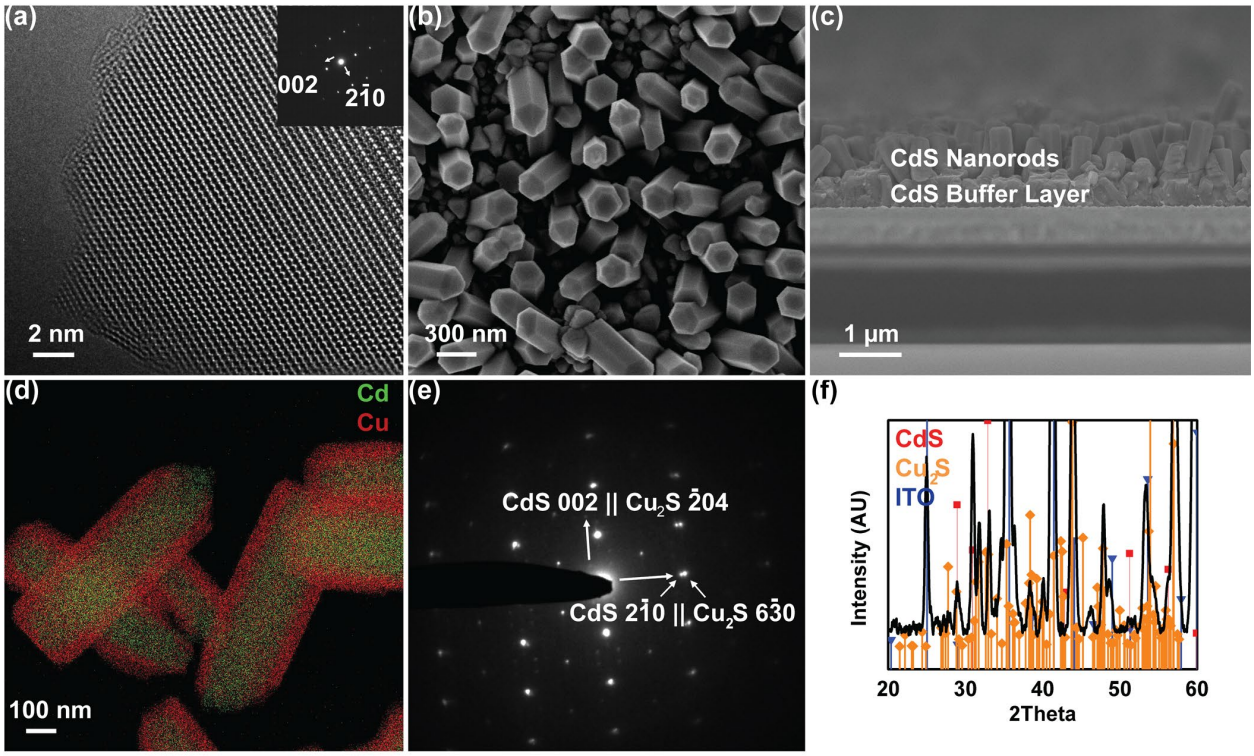

Figure 1. Characterization of the CdS nanorods used for the cation exchange reaction and Cu_2S after conversion of CdS nanorods. (a) HRTEM image of an individual CdS nanorod with inset diffraction pattern. (b) Top-view SEM image of a CdS nanorod array. (c) Cross-sectional SEM image of a CdS nanorod array showing the interface with the underlying FTO substrate. (d) Energy dispersive X-ray spectroscopy (EDS) images of partially converted CdS-Cu_2S nanorods synthesized under the same conditions used for photovoltaic devices. Cadmium is shown in green, and copper is shown in red. (e) Selected area diffraction pattern of a core-shell CdS-Cu_2S nanorod. (f) X-ray diffraction pattern of CdS-Cu_2S core-shell nanorods indicating the presence of wurtzite CdS (red squares) as well as low-chalcocite Cu_2S (orange diamonds). Diffraction peaks from ITO substrate are also shown (blue triangles).

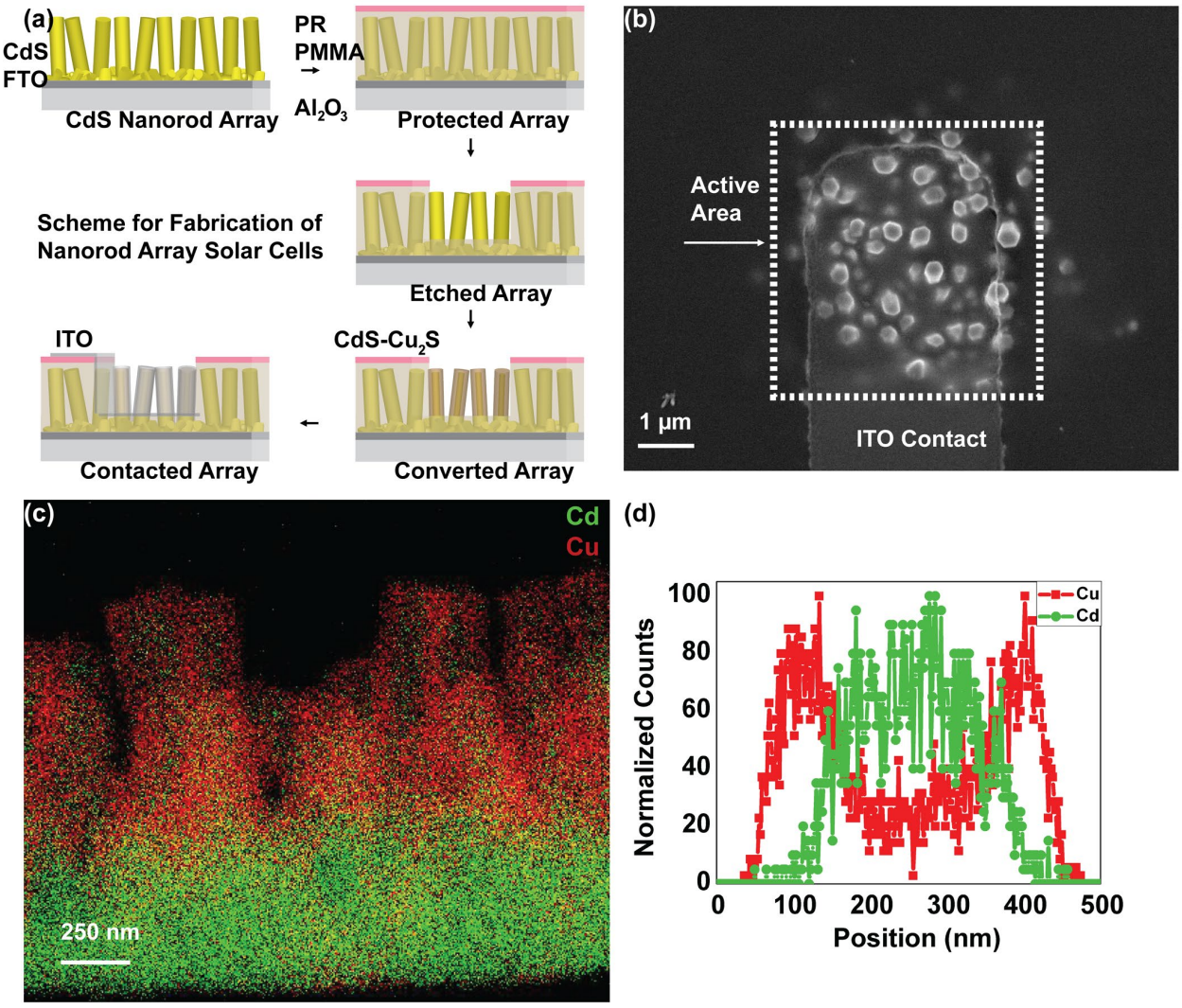

Figure 2. Fabrication of photovoltaic devices from CdS nanorod arrays. (a) Schematic of the device fabrication process. (b) SEM image of the active area of a finished device. (c) A cross-sectional EDS map demonstrating that the underlying layer of particles consists of CdS after protection with PMMA and cation exchange of the nanorods above. (d) EDS line scan of a single nanorod showing the measured Cu_2S shell thickness on the CdS core.

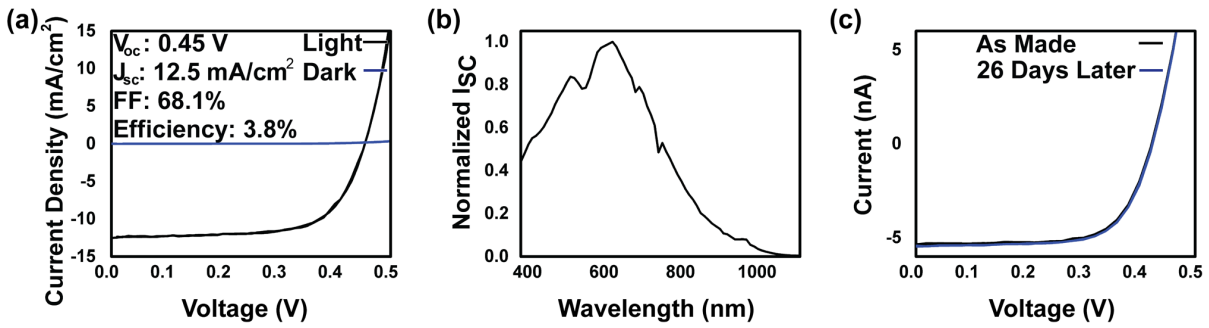

Figure 3. Characterization of the performance of CdS-Cu_2S core-shell nanorod array devices. (a) *J-V* characteristic of a champion core-shell nanorod array solar cell in the dark and under 1-sun (AM 1.5G) illumination. (b) Short-circuit current normalized by photon flux as a function of wavelength of light showing a strong contribution from the Cu_2S beyond the absorption edge of CdS at approximately 520 nm. (c) *I-V* characteristic of a core-shell nanorod array solar cell under 1-sun (AM 1.5G) illumination after fabrication and 26 days later after storage in air.

ASSOCIATED CONTENT

Supporting Information. Detailed protocols for nanorod growth and solar cell fabrication, SEM image of CdS nanorod array after protection by PMMA, table of representative functional devices, photoluminescence of CdS, and UV-vis spectra. This material is available free of charge via the Internet at http://pubs.acs.org.

AUTHOR INFORMATION

Corresponding Author

Address correspondence to p_yang@berkeley.edu.

Present Addresses

¶Present address for N. P. Dasgupta: Department of Mechanical Engineering, University of Michigan, Ann Arbor, Michigan 48109, United States

Author Contributions

The manuscript was written through contributions of all authors. All authors have given approval to the final version of the manuscript.

Notes

The authors declare no competing financial interests.

Funding Sources

This work was supported by the Bay Area Photovolatic Consortium, DOE prime award number DE-EE0004946 and sub-award number 60094384-51077-D.

ACKNOWLEDGMENT

The authors thank the National Center for Electron Microscopy at the Molecular Foundry in Lawrence Berkeley National Laboratory. Work at the Molecular Foundry was supported by the Office of Science, Office of Basic Energy Sciences, of the U.S. Department of Energy under Contract No. DE-AC02-05CH11231). Special thanks to Dr. Anthony Fu and Dr. Letian Dou for helpful scientific discussions.

REFERENCES

1. Rothwarf, A. *Sol. Cells*, **1972**, 2, 115-140.
2. Henry, C. H. *J. Appl. Phys*. **1980**, 51, 4494-4500.
3. Beberwyck, B. J.; Surendranah, Y.; Alivisatos A. P. *J. Phys. Chem. C* **2013**, 117, 19759-19770.

4. Rivest, J. B.; Jain P. K. *Chem. Soc. Rev*. **2013**, 43. 89-96.

5. Deka, S.; Miszta, K.; Dorfs, D.; Genovese, A.; Bertoni, G.; Manna, L. *Nano Lett*. **2010**, 10, 3770−3776.

6. Eggleston, A. W.; Moses, M. J. *Sol. Cells*, **1985**, 14, 1-11.

7. Bragagnolo, J. A.; Barnett, A. M.; Phillips, J. E.; Hall, R. B.; Rothwarf, A.; Meakin, J. D. *IEEE Trans*. *Electron Devices* **1980**, 27, 645−651.

8. Riha, S. C.; Jin, S.; Baryshev, S. V.; Thimsen, E.; Wiederrecht, G. P.; Martinson, A. B. F. *ACS Appl*. *Mater*. *Interfaces* **2013**, 5, 10302-10309.

9. Green, M. A. *Prog. Photovoltaics Res. Appl.* **2009**, 17, 183-189.

10. Norian, K. H.; Edington, J. W. *Thin Solid Films* **1981**, 75, 53-65.

11. Al-Dhafiri, A. M.; Russell, J. G.; Woods, J. *Semicond. Sci. Technol.* **1992**, 7, 1052-1057.

12. Martinson, A. B. F.; Riha S. C.; Thimsen, E.; Elam, J. W.; Pellin M. J. *Energy Environ*. *Sci*. **2013**, 6, 1868-1878.

13. Dasgupta, N. P.; Sun, J.; Liu, C.; Brittman, S.; Andrews, S. C.; Lim, J.; Gao, H.; Yan, R.; Yang, P. *Adv. Mater.* **2014**, 26, 2137-2184.

14. Tang, J.; Huo, Z.: Brittman, S; Gao, H.; Yang, P. *Nat. Nanotechnol.* **2011**, 6, 568-572.

15. Garnett, E. C.; Brongersma, M. L.; Cui, Y; McGehee, M. D. *Annu. Rev. Mater. Res.* **2011**, 41, 269-295.

16. Kayes, B. M.; Atwater, H. A.; Lewis, N. S. *J. Appl. Phys.* **2005**, 97, 114302-114311.

17. Kelzenberg, M. D.; Boettcher, S.W.; Petykiewicz, J. A.; Turner-Evans, D. B.; Putnam, M. C.; Warren, E. L.; Spurgeon, J. M.;. Briggs, R. M. Lewis, N. S.; Atwater, H. A. *Nat. Mater.* **2010**, 9, 239-244.

18. Muskens, O. L.; Rivas, G. R.; Algra, R. E.; Bakkers, E. P. A. M.; Lagendijk, A. *Nano Lett.* **2008**, 8, 2638-2642.

19. Garnett, E.; Yang, P. *Nano Lett.* **2010**, 10, 1082-1087.

20. Fan, Z.; Razavi, H.; Do, J.-W.; Moriwaki, A.; Ergen, O.; Chueh, Y.-L.; Leu, P. W.; Ho, J. C.; Takahashi, T.; Reichertz, J. A.; Neale, S.; Yu, K.; Wu, M.; Ager, J. W., Javey, A. *Nat. Mater.* **2009**, 8, 648-653.

21. Hongyu, S.; Li, X.; Chen, Y.; Guo, D.; Xie, Y.; Li, W.; Liu, B.; Zhang, X. *Nanotechnology* **2009,** 20, 425603.

22. Lee, J.-C.; Lee, W.; Han, S.-H. Kim, T. G.; Sung, Y. M. *Electrochem. Commun.* **2009**, 11, 231-234.

23. Sadtler, B.; Demchenko, D. O.; Zheng, H.; Hughes, S. M.; Merkle, M. G.; Dahmen, U.; Wang, L. W.; Alivisatos, A. P. *J. Am. Chem. Soc.* **2009**, 131, 5285−5293.

24. Zhang, D.; Wong, A. B.; Yu, Y., Brittman, S.; Sun, J.; Fu, A.; Beberwyck, B.; Alivisatos, A. P., Yang, P. *J. Am. Chem. Soc.* **2014**, 136, 17430–17433.

25. Rivest, J. B.; Swisher, S. L.; Fong, L. K.; Zheng, H.; Alivisatos A. P. *ACS Nano* **2011**, 5, 3811−3816.

26. Chen, F.; Qiu, W.; Chen, X.; Yang, L.; Jiang, X.; Wang, M.; Chen, H. *Sol. Energy* **2011**, 85, 2122–2129.

27. Sun, M.; Fu, W.; Li, Q.; Yin, G.; Chi, K.; Zhou, X.; Ma, J.; Yang, L.; Mu, Y.; Chen, Y.; Yang, H. *J. Cryst. Growth* **2012,** 377, 112–117.

28. Pan, C.; Niu, S.; Ding, Y.; Dong, L.; Yu, R.; Liu, Y.; Zhu, G.; Wang, Z. L. *Nano Lett.* **2012**, 3302−3307.

29. Aperathitis, E.; Bryant, F. J.; Scott, C. G. *Sol. Cells* **1990**, 28, 261 – 272.

30. Gill, W.; Bube, R. *J. Appl. Phys*. **1970**, 41, 3731-3738.

31. Wu, Y.; Wadia, C.; Ma, W.; Sadtler, B.; Alivisatos, A. P. *Nano Lett.* **2008**, 8, 2551-2554.

32. Zheng, H.; Sadtler, B.; Habenicht, C.; Freitag, B.; Alivisatos, A. P., Kisielowski, C. *Ultramicroscopy* **2013**, 134, 207-213.

33. Wang, S.; Yang, S. *Chem. Phys. Lett.* **2000**, 322, 567-571.

TOC: